Research Article

Journal of Environmental Nanotechnology

# Nano-reinforcement and Synthesis of Al 8090-based Hybrid Composites with $B_4C$ and Coconut Shell Charcoal for Enhanced Tribological Performance

B. Silambarasan[1*], Sugavanam Janakiraman[2], Rajabharathi Balavadivel[2] and Gokulkumar Sivanantham[3]

[1]Department of Mechanical Engineering, Sir Issac Newton College of Engineering and Technology, Nagapattinam, TN, India
[2]Department of Mechanical Engineering, Academy of Maritime Education and Training (Deemed to be University), Chennai, TN, India
[3]Department of Mechanical Engineering, KPR Institute of Engineering and Technology, Coimbatore, TN, India
Received: 09.07.2025 Accepted: 16.09.2025 Published: 30.09.2025
*balasilambu05@gmail.com

## ABSTRACT

This study investigates the tribological properties of Aluminum 8090-based hybrid composites reinforced with 3 wt. % $B_4C$ and varying weight percentages (2%, 3%, and 4%) of coconut shell charcoal (CSC) nanoparticles. The composites were fabricated using stir casting and characterized for their density, porosity, hardness, and wear behavior under different operating conditions. The density decreased with increasing CSC content, whereas the porosity remained below 2.37%, indicating effective particle dispersion. The hardness improved with higher CSC loading, reaching 133.1 HV for the 4% CSC composite. Tribological tests were conducted using a pin-on-disk tribometer, varying the applied load (10, 20, and 30 N), temperature (27, 50, and 100 °C), and sliding distance (500, 1000, and 1500 m). The Taguchi method and ANOVA revealed that the sliding distance was the most influential factor for both the wear rate and coefficient of friction (COF), followed by the CSC content. The optimal conditions for minimal wear (0.01422 $mm^3/m$) and COF (0.449) were found to be 10 N, 27 °C, 2% CSC, and 500 m. The 4% CSC composite exhibited the best overall performance, with low porosity (1.99%), high hardness (133.1 HV), and a reduced COF (0.406). The SEM-EDS analysis confirmed the uniform dispersion of the $B_4C$ and CSC reinforcements within the Al 8090 matrix, with minimal porosity and strong interfacial bonding. The results highlight the potential of Al 8090/$B_4C$/CSC hybrid composites for applications requiring high wear resistance and low friction, such as in aerospace and automotive components.

**Keywords:** Tribological properties; Aluminum 8090; Hybrid composites; Boron carbide; Coconut shell charcoal; Stir casting; Taguchi method.

## 1. INTRODUCTION

Metal Matrix Composites (MMCs) have emerged as advanced materials with exceptional mechanical and tribological properties, making them highly suitable for demanding applications in industries such as aerospace (Pattar *et al.* 2024), automotive (Dwivedi *et al.* 2022), and defense (Siengchin, 2023). Aluminum-based MMCs are particularly valued for their high strength-to-weight ratio, enhanced stiffness, and superior wear resistance, which are critical for components subjected to harsh operating conditions (Kumar *et al.* 2022). The choice of matrix material heavily influences the properties of MMCs (Karthikeyan *et al.* 2020; Prakash and Das, 2021), reinforcement type (Kar and Surekha, 2019; Arunkumar and Kumar, 2022), and fabrication technique (Subramaniam *et al.* 2019; Harish *et al.* 2023). Among the various fabrication methods, stir casting, a liquid-state processing technique, is widely adopted because of its cost-effectiveness and ability to minimize casting defects. This study focuses on Aluminum 8090 (Al 8090), a lithium-based wrought alloy known for its excellent strength and durability, particularly in high-performance applications. Aluminum 8090 alloy was selected as the matrix material due to its unique combination of properties compared to other widely used aluminum alloys, such as Al 6061 and Al 7075. It offers a significantly lower density, which improves the strength-to-weight ratio, an essential factor for aerospace and automotive applications. Moreover, its high stiffness, good fatigue resistance, and superior corrosion behavior make it more suitable for high-performance environments than conventional alloys. However, by incorporating ceramic reinforcements such as $B_4C$ (Hynes *et al.* 2020; Asha *et al.* 2021) and sustainable, bio-derived coconut shell charcoal (CSC) nanoparticles (Raju *et al.* 2018; Ravi *et al.* 2018; Yekinni *et al.* 2020; Lokeshwari *et al.* 2022), this study aimed to develop hybrid composites with enhanced tribological and mechanical properties. Among various biomass-derived reinforcements, CSC nanoparticles present unique advantages that distinguish them from alternatives such as rice husk ash, palm kernel shell ash, or cow dung ash. Owing to their high carbon content and

porous microstructure, CSC particles act not only as a lightweight reinforcement but also as a solid lubricant by forming a protective tribo-layer during sliding, thereby reducing wear and friction more effectively than silica- or oxide-rich ashes. Their intrinsically low density (1.4–1.6 g/cm$^3$) further enhances the lightweighting effect of aluminum composites, which is particularly valuable for aerospace and automotive applications. Moreover, the carbonaceous nature of CSC contributes to improved thermal stability at elevated temperatures, ensuring better retention of tribological performance compared to other biomass-based reinforcements. In addition to these functional benefits, CSC is abundantly available as an agricultural by-product in tropical regions, making its use both cost-effective and eco-friendly. These unique features underscore the novelty of CSC as a reinforcement material for developing sustainable, high-performance aluminum matrix composites. Similarly, $B_4C$ is a preferred reinforcement due to its exceptional hardness, chemical compatibility with aluminium, and high thermal conductivity. Halil *et al.* (2019) investigated Al6082/SiC/ $B_4C$ hybrid composites, reporting improved hardness and wear resistance due to the synergistic effect of dual reinforcements. The use of bio-derived reinforcements, such as coconut shell charcoal, has become widely used (Subramaniam *et al.* 2018). Likewise, Sudhakar *et al.* (2025) utilized powder metallurgy to fabricate AA7075/$B_4C$/ZrC hybrid composites, achieving enhanced hardness and wear resistance through the precise control of the particle distribution. The combination of these reinforcements is expected to offer a unique synergy and the thermal stability of CSC to optimize the performance under various operating conditions, including elevated temperatures and varying loads.

Aluminum-based MMCs reinforced with ceramic particulates such as SiC, $Al_2O_3$, and $B_4C$ have been extensively studied for their improved mechanical properties, including hardness, tensile strength, and wear resistance (Manikandan *et al.* 2020; Silambarasan and Karthikeyan, 2023). Akgümüş *et al.* (2024) reviewed the reinforcement philosophies for aluminum hybrid composites. They highlighted that the addition of hard ceramic particles enhances the strength by impeding dislocation movement within the matrix, leading to improved wear resistance suitable for automotive and aerospace applications. Similarly, Oza *et al.* (2021) investigated the wear characteristics of Al/SiC/graphite hybrid composites and noted that the incorporation of dual reinforcements reduced the wear rate compared to single-reinforced composites owing to the improved load-bearing capacity and lubricity. Adediran *et al.* (2020) explored the mechanical and wear behaviors of Al-based composites reinforced with steel and graphite, reporting enhanced dimensional stability and corrosion resistance, which are critical for marine applications. These studies underscore the potential of hybrid reinforcements to tailor composite properties for specific applications, although most investigations have been conducted under ambient conditions only.

The fabrication method significantly influences the performance of aluminum MMCs. Stir casting is a versatile and cost-effective liquid-state processing technique that ensures the uniform dispersion of reinforcements, minimizing defects such as porosity (Mahanta *et al.* 2019; Pawar and Kharde, 2021; Arunkumar *et al.* 2020; Karpasand *et al.* 2020). Bhowmik *et al*. (2024) demonstrated that stir-cast Al7075-$TiB_2$ composites exhibited superior tribological properties owing to the strong interfacial bonding between the matrix and reinforcement. Sharma *et al.* (2024) compared liquid- and solid-state processing, noting that stir casting offers scalability, whereas powder metallurgy provides better control over the microstructure. These studies highlight the importance of fabrication techniques in achieving optimal reinforcement dispersion and composite performance improvements.

Satheesh and Pugazhvadivu, (2019) studied Al6061-CSA composites, noting that CSC reinforcement reduced density while maintaining adequate mechanical strength. Poornesh *et al.* (2024) explored Al-Si-Fe/CSC composites and found that CSC improved wear resistance by forming a protective tribo-layer during sliding (Lan *et al.* 2022). These studies indicate that combining $B_4C$ with bio-derived reinforcements, such as CSC, can enhance composite properties while promoting eco-friendly material development. Sharma *et al.* (2021) examined Al6061-based composites reinforced with hematite and titania, noting a significant increase in wear rate at higher temperatures due to matrix softening. Pawar *et al.* (2023) investigated LM26/SiC/Ni-Gr composites and reported that the formation of tribo-layers at elevated temperatures mitigated wear to some extent.

Despite extensive research on aluminum-based MMCs, most studies have focused on single or dual ceramic reinforcements under ambient conditions, with limited attention to hybrid composites incorporating sustainable reinforcements such as CSC at elevated temperatures. The synergistic effects of $B_4C$ and CSC in Al 8090 matrices, particularly in terms of tribological performance under varying loads, temperatures, and sliding distances, have not been investigated thoroughly. Furthermore, the use of statistical tools, such as the Taguchi method, to optimize the wear rate and coefficient of friction (COF) in such hybrid systems is scarce. This study aims to address these gaps by systematically evaluating the tribological properties of Al 8090-based hybrid composites reinforced with $B_4C$ and CSC under diverse operating conditions, providing insights into their performance and optimization.

This study focused on the development and characterization of Al 8090-based hybrid composites

reinforced with 3 wt. % $B_4C$ and varying weight percentages (0%, 2%, 3%, and 4%) of CSC nanoparticles, fabricated *via* stir casting. The scope includes evaluating the mechanical properties (hardness, tensile strength, and density) and tribological behavior (wear rate and COF) under different operating conditions, including applied load (10, 20, and 30 N), temperature (27, 50, and 100°C), and sliding distance (500, 1000, and 1500 m). The Taguchi method and ANOVA were employed to identify the most influential parameters affecting wear performance and to optimize the composite composition for minimal wear rate and COF. Microstructural analysis using SEM, EDS, and XRD provides insights into reinforcement dispersion and wear mechanisms, contributing to the development of high-performance, sustainable composites.

The primary objectives of this study were as follows:

- To fabricate Al 8090-based hybrid composites with 3 wt. % $B_4C$ and varying CSC content (2%, 3%, and 4%) using the stir casting technique.
- To evaluate the mechanical properties, including the hardness and density, of the fabricated composites.
- To investigate the tribological properties (wear rate and COF) under varying operating conditions, including applied load, temperature, and sliding distance.
- To employ Taguchi method and ANOVA to identify the most influential factors affecting wear performance and to optimize the composite composition.
- To analyze the microstructural characteristics and wear mechanisms using SEM, EDS, and XRD to understand the role of reinforcements in enhancing the composite performance.

Al 8090-based hybrid composites reinforced with $B_4C$ and CSC have significant potential for various high-performance applications. In the automotive industry, these composites can be used to manufacture piston seats, brake rotors, and engine components because of their high wear resistance, low density, and thermal stability. In aerospace applications, the high strength-to-weight ratio and corrosion resistance of composites make them suitable for structural components such as aircraft frames and landing gear. The defense sector can benefit from these materials in lightweight armor and weapon systems, where durability and impact resistance are critical factors. Additionally, the use of sustainable CSC reinforcement aligns with eco-friendly manufacturing practices, making these composites attractive for marine applications, such as propeller shafts and hull components, where corrosion and wear resistance are essential properties. Optimized tribological performance at elevated temperatures further broadens their applicability in high-temperature environments, such as turbine blades and exhaust systems.

## 2. MATERIALS AND METHODS

### 2.1 Materials - Aluminium (Al 8090), Boron Carbide ($B_4C$), and Coconut Shell Charcoal (CSC) Nanoparticles

In this study, hybrid Metal Matrix Composites (MMCs) were developed by customizing Aluminium 8090 (Al 8090) alloy reinforced with $B_4C$ and coconut shell charcoal (CSC) nanoparticles. The mechanical and tribological properties of these composites were systematically evaluated to assess their performance under various conditions. Al 8090 (with a density of 2.54 g/cm³ and a melting point of 600 – 655 °C) is a lithium-based wrought alloy renowned for its excellent strength-to-weight ratio and durability, making it suitable for applications in aerospace, cryogenic temperature services, and defense systems. The alloy was procured from Bharat Aerospace Metals (Mumbai, India). Its chemical composition, as shown in Table 1, enables effective strengthening mechanisms, making it an ideal matrix material for multiparticle-reinforced MMCs.

$B_4C$ nanoparticles, with a particle size of approximately 10 µm and a density of 2.52 g/cm$^3$, were sourced from Bharat Aerospace Metals, Mumbai, India. $B_4C$ is known for its exceptional hardness, high melting point, and chemical inertness, making it an ideal reinforcement for enhancing the mechanical and tribological properties of aluminum-based composites.

**Table 1: Chemical composition of aluminium 8090 alloy**

| Element | Li | Cu | Mg | Fe | Zn | Si | Ti, Cr, Mn | Zr | Al |
|---|---|---|---|---|---|---|---|---|---|
| % of Composition | 2.2-2.7 | 1-1.6 | 0.6-1.3 | 0.30 | 0.25 | 0.20 | 0.10 | 0.04-0.16 | 93-96.2 |

Coconut shell charcoal (CSC) nanoparticles were prepared from dried coconut shells. The shells were collected, crushed into a coarse powder using a jaw crusher, and milled using a hammer mill. The resulting powder was subjected to heat treatment in an argon gas atmosphere at 1150°C for three hours to produce CSC ash. The ash was then filtered and ground in a ball mill to achieve fine nanoparticle sizes suitable for

reinforcement. The use of CSC provides a sustainable, low-density reinforcement option, contributing to the development of eco-friendly composites.

## 2.2 Preparation of Composite

The hybrid composites were fabricated using the stir casting technique, as shown in Fig. 1, and compositions as per Table 2. Al 8090 alloy was melted in a graphite crucible within an electric resistance furnace under a protective atmosphere of 98% argon and 2% $SF_6$ to prevent oxidation. $B_4C$ particles were preheated to 400 °C and CSC nanoparticles were heat-treated to remove moisture and improve wettability before being gradually added to the molten alloy. The mixture was stirred at 600 rpm for 15 min using a graphite-coated impeller to promote homogeneous particle distribution and minimize agglomeration. The melt was then poured into a steel mold preheated to 300 °C, reducing thermal gradients and casting defects. The solidified composites were cooled under controlled conditions and machined into test specimens in accordance with ASTM standards. These measures collectively ensured effective dispersion and strong interfacial bonding between the reinforcements and the matrix, as confirmed by SEM–EDS analysis.

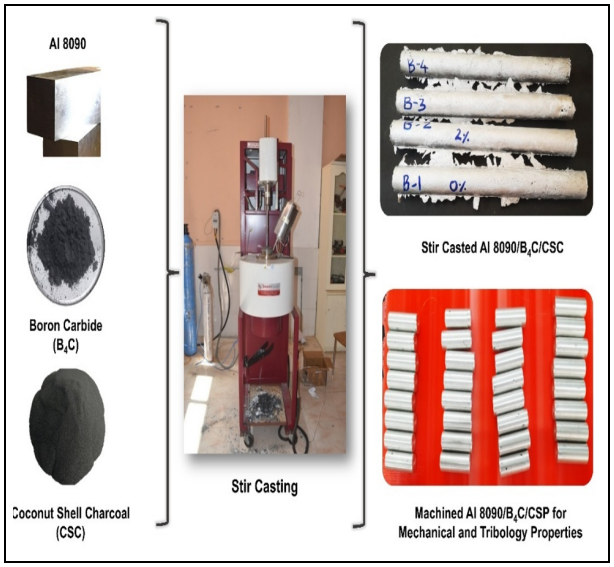



**Fig. 1: Schematic of stir casting setup for fabricating Al 8090 hybrid composites**

## 2.3 Material Characterization

### 2.3.1 Density and Porosity Measurement

The density of the composite samples was measured using Archimedes' principle with a high-precision digital electronic balance (accuracy of 0.0001 g), according to the ASTM B962-08 standard. Theoretical densities were calculated using the rule of mixtures, and porosity was estimated by comparing the theoretical and actual density values.

### 2.3.2 Hardness Test

The Vickers hardness of the composite samples was measured using a Micro-Vickers Hardness Tester, following the ASTM E-384 standards. A load of 200 g was applied for 15 s at five different locations on each sample, and the average hardness value was computed.

### 2.3.3 Wear Test and Design of Experiments (DOE)

The tribological properties of the composites were evaluated using a pin-on-disk tribometer, as shown in Fig. 2. The wear tests were carried out under dry sliding conditions without the use of any external lubrication, in order to simulate severe service environments. Wear debris generated during sliding was allowed to evacuate naturally from the contact surface. To minimize interference from accumulated particles, the pin and disk surfaces were thoroughly cleaned with acetone and dried before each test run. This ensured consistency and prevented residual debris from influencing subsequent measurements. The Design of Experiments (DOE) approach was employed to systematically investigate the effects of key parameters on the wear rate and COF. The parameters studied were the applied load, temperature, weight percentage of CSC, and sliding distance, with their respective levels shown in Table 3.

**Table 2. Compositions of Al 8090-based hybrid composite samples**

| Composite Samples | Wt. % of Al 8090 | Wt. % of $B_4C$ | Wt. % of CSC |
|---|---|---|---|
| Sample A (Al8090+3% $B_4C$+2% CSC) | 95 | 3 | 2 |
| Sample B (Al8090+3% $B_4C$+3% CSC) | 94 | 3 | 3 |
| Sample C (Al8090+3% $B_4C$+4% CSC) | 93 | 3 | 4 |

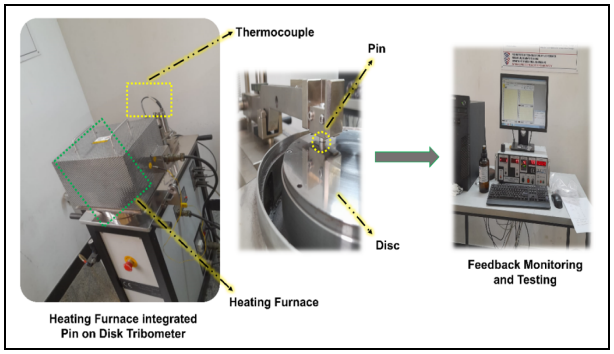



**Fig. 2: Pin-on-disk tribometer used for wear and friction testing**

The Taguchi design of experiments and subsequent ANOVA were performed using Minitab 22 statistical software. An L9 orthogonal array (Table 4) was

selected within the software framework to accommodate the four control factors (applied load, temperature, CSC content, and sliding distance), each at three levels. The choice of this array was validated by confirming that the degrees of freedom for the selected design exceeded the total degrees of freedom of the factors, ensuring adequate coverage of parameter interactions. Signal-to-noise (S/N) ratios were calculated using the 'smaller-the-better' criterion to minimize wear rate and coefficient of friction. The orthogonal array and S/N ratio selection were further verified through Minitab's built-in model adequacy checks, ensuring statistical validity and reproducibility of the experimental design.

**Table 3. Experimental parameters and levels for wear testing**

| Parameter | Unit | Level 1 | Level 2 | Level 3 |
|---|---|---|---|---|
| Applied load | N | 10 | 20 | 30 |
| Temperature | ℃ | 27 | 50 | 100 |
| Weight % of CSC | Wt. % | 2 | 3 | 4 |
| Sliding Distance | m | 500 | 1000 | 1500 |

**Table 4. Taguchi L9 orthogonal array used for DOE**

| Trial Run | Applied load (N) | Temperature (℃) | Wt. % of CSC |
|---|---|---|---|
| 1 | 10 | 27 | 2 |
| 2 | 10 | 50 | 3 |
| 3 | 10 | 100 | 4 |
| 4 | 20 | 27 | 3 |
| 5 | 20 | 50 | 4 |
| 6 | 20 | 100 | 2 |
| 7 | 30 | 27 | 4 |
| 8 | 30 | 50 | 2 |
| 9 | 30 | 100 | 3 |

#### 2.3.4 X-ray Diffraction (XRD) Analysis

The phase composition and crystal structure of the Al 8090-based hybrid composites were analyzed using a D8 ADVANCE X-Ray Diffractometer (XRD) (Bruker). This instrument was employed to identify the presence of Al 8090, $B_4C$, and coconut shell charcoal (CSC) phases, as well as any secondary phases formed during the stir casting process. XRD analysis was conducted using Cu Kα radiation (λ = 1.5406 Å) at a scan rate of 2°/min over a 2θ range of 10° to 90°. The resulting XRD patterns were normalized to determine the relative intensities of the peaks, providing insights into the chemical composition, phase distribution, and crystallinity of the composites. These data confirmed the uniform incorporation of $B_4C$ and CSC reinforcements within the Al 8090 matrix and detected any interfacial reaction products.

#### 2.3.5 Scanning Electron Microscopy (SEM) and Energy Dispersive Spectroscopy (EDS)

Microstructural analysis of the hybrid composites was performed using a Carl Zeiss Sigma 300 field-emission scanning electron microscope (FE-SEM) equipped with a Smart EDX energy-dispersive X-ray spectroscopy (EDS) system. The Sigma 300 FE-SEM offers a resolution of 1.0 nm at 15 kV and 1.6 nm at 1 kV, with an acceleration voltage range of 0.02–30 kV and magnification capabilities up to 1,000,000x. SEM imaging was used to examine the dispersion of $B_4C$ and CSC nanoparticles within the Al 8090 matrix and to assess the interfacial bonding and potential defects, such as voids or agglomeration. The Smart EDX system facilitated elemental mapping and quantitative analysis, confirming the distribution of aluminum, boron, carbon, and other elements present in the composite. This analysis provides critical insights into the homogeneity of the reinforcement distribution and the integrity of the matrix-reinforcement interface.

## 3. RESULTS AND DISCUSSIONS

### 3.1 Density and Porosity Values of Al 8090-based Hybrid Composites

The density and porosity of the Al 8090-based hybrid composites shown in Table 5, reinforced with 3 wt. % $B_4C$ and varying CSC content (2%, 3%, and 4%), were investigated to evaluate the effect of CSC reinforcement on the physical properties of the composites. The theoretical density, determined using the rule of mixtures, decreased from 2.5405 g/cm$^3$ for Sample A (Al 8090 + 3% $B_4C$ + 2% CSC) to 2.5319 g/cm$^3$ for Sample C (Al 8090 + 3% $B_4C$ + 4% CSC), driven by the lower intrinsic density of CSC (1.4–1.6 g/ cm$^3$) compared to Al 8090 (2.54 g/cm³) and $B_4C$ (2.52 g/ cm$^3$). The actual density, measured via Archimedes' principle per ASTM B962-08 using a high-precision digital balance (0.0001 g accuracy), followed a similar trend, declining from 2.4810 g/ cm$^3$ in Sample A to 2.4816 g/ cm$^3$ in Sample C. This reduction, ranging from 0.17% to 0.34% in theoretical density, highlights CSC's role in producing lightweight composites suitable for aerospace and automotive applications. The porosity, calculated as the percentage difference between the theoretical and actual densities, ranged from 1.99% to 2.37%. Sample A exhibited a porosity of 2.34%, which slightly increased to 2.37% in Sample B (3% CSC), likely due to CSC's porous microstructure of CSC and potential challenges in achieving uniform dispersion during stir casting, despite the use of a protective atmosphere (98% argon, 2% sulfur hexafluoride) and a preheated mold (300℃). The increase in porosity may also arise from weaker interfacial bonding between the CSC and Al 8090 matrix or minor gas entrapment during stirring at 600 rpm. Notably, Sample C (4% CSC) exhibited a reduced porosity of 1.99%, suggesting improved particle packing

or agglomeration at higher CSC content, possibly aided by preheating the CSC to 400°C to minimize moisture-related defects. These porosity levels, remaining below 2.37%, indicate effective stir casting parameters compared to studies (Silambarasan and Karthikeyan, 2023) which reported higher porosity with bio-based reinforcements. The slight increase in porosity in Sample B could influence mechanical properties, such as tensile strength, owing to stress concentrations at the voids; however, the low overall porosity suggests minimal defects. Regarding tribological performance, the higher porosity of Sample B may affect the surface integrity, although the hardness of $B_4C$ and CSC's potential lubricity could counteract wear. The reduction in porosity at 4% CSC was associated with better packing at higher ash content in Al 6061 composites. To further optimize the density and porosity, future studies could explore enhanced stirring techniques, CSC surface treatments for improved wettability, or adjusted $B_4C$-to-CSC ratios to balance lightweight properties with structural integrity for high-performance applications.

**Table 5. Density and porosity values of hybrid composites**

| S. No. | Description | Theoretical Density ($g/cc^3$) | Actual Density ($g/cc^3$) | Porosity (%) |
|---|---|---|---|---|
| 1 | Sample A (Al8090 + 3% $B_4C$ + 2% CSC) | 2.5405 | 2.4810 | 2.34 |
| 2 | Sample B (Al8090 + 3% $B_4C$ + 3% CSC) | 2.5362 | 2.4762 | 2.37 |
| 3 | Sample C (Al8090 + 3% $B_4C$ + 4% CSC) | 2.5319 | 2.4816 | 1.99 |

## 3.2 Vickers Hardness Values of Al 8090-based Hybrid Composites

The Vickers hardness of the Al 8090-based hybrid composites (Table 6), reinforced with 3 wt. % Boron Carbide ($B_4C$) and varying coconut shell charcoal (CSC) content (2%, 3%, and 4%) were measured to evaluate the effect of CSC reinforcement on the mechanical properties of the composites. Hardness tests were conducted using a Micro-Vickers Hardness Tester, following ASTM E-384 standards, with a load of 200 g applied for 15 s at five different locations on each sample, and the average hardness values were computed. The results showed that Sample A (Al 8090 + 3% $B_4C$ + 2% CSC) exhibited a hardness of 127.6 HV, which increased to 129.3 HV for Sample B (3% CSC) and 133.1 HV for Sample C (4% CSC). The progressive increase in hardness with higher CSC content can be attributed to several synergistic mechanisms. First, the uniform dispersion of CSC particles at higher loadings improves particle–matrix interlocking, which restricts plastic deformation. Second, the reduction in porosity at 4% CSC (1.99%) minimizes weak points within the matrix, thereby enhancing load-bearing capacity. Third, CSC contributes to load transfer, as the hard particles absorb part of the applied stress, increasing the resistance to indentation. Finally, the combination of CSC with $B_4C$ provides a dual reinforcement effect, where $B_4C$ impedes dislocation motion and CSC enhances dispersion hardening, together resulting in superior hardness.

In contrast, CSC, despite its lower intrinsic strength, contributed to the hardness at higher loadings, likely owing to the increased particle-matrix interlocking and reduced void formation, as supported by the lower porosity (1.99%) observed in Sample C than in Samples A (2.34%) and B (2.37%). The initial lower hardness of Sample A may result from suboptimal CSC dispersion or weaker interfacial bonding at 2% CSC, which improved with increasing CSC content, as evidenced by the 4.3% increase in hardness from Sample A to Sample C. Compared to the literature, such as Singh *et al*. (2016), who reported enhanced hardness in Al-based composites with $B_4C$ and SiC, the addition of CSC appears to provide a complementary effect. However, its contribution is less dominant than that of $B_4C$ owing to its bi-derived, less complex nature. The hardness values remain lower than those of Al 8090 reinforced solely with 3% $B_4C$ (139.7 HV, as previously reported), indicating that the CSC slightly dilutes the hardening effect of $B_4C$ but offers benefits in reducing density. The observed trend suggests that 4% CSC (Sample C) approaches an optimal balance, enhancing the hardness while maintaining lightweight properties, which is critical for applications in aerospace and automotive components. Future improvements could involve optimizing the CSC particle size or surface treatments to enhance wettability and bonding with the Al 8090 matrix, potentially further increasing the hardness while minimizing porosity-related drawbacks.

## 3.3 Tribological Analysis of Al 8090-based Hybrid Composites

The tribological performance of Al 8090-based hybrid composites (Table 7) reinforced with 3 wt. % Boron Carbide ($B_4C$) and varying coconut shell charcoal (CSC) content (2%, 3%, and 4%), was evaluated using a pin-on-disk tribometer to assess wear rate and coefficient of friction (COF) under varying conditions of applied load (10–30 N), temperature (27–100°C), sliding distance (500–1500 m), and CSC weight percentage. A DOE approach, utilizing the Taguchi L9 orthogonal array generated by Minitab 22 software, was employed to investigate the influence of these parameters systematically. The "smaller the better" criterion was applied to the signal-to-noise (S/N) ratio to minimize the wear rate and COF, and ANOVA was conducted to quantify the contribution of each factor. Regression equations were developed to model the relationships between the input parameters and tribological responses.

Among the tested parameters, sliding distance exerted the strongest influence on both wear rate and COF, as prolonged sliding significantly increases cumulative abrasive and adhesive interactions, allowing wear debris to accumulate and accelerate material loss. In contrast, applied load and temperature showed comparatively lesser effects. Although higher loads increase contact stress and elevated temperatures soften the Al 8090 matrix, these effects were mitigated by the synergistic action of $B_4C$ and CSC reinforcements: $B_4C$ provided hardness and load-bearing capability, while CSC formed a lubricious tribo-layer that reduced frictional heating and protected the surface. Consequently, while load and temperature influenced wear behavior, their impact was secondary to the dominant effect of sliding distance.

**Table 6: Vickers hardness of composites with varying CSC content**

| S. No. | Sample Description | Vickers Hardness (HV) |
|---|---|---|
| 1 | Sample A (Al8090 + 3% $B_4C$ + 2% CSC) | 127.6 |
| 2 | Sample B (Al8090 + 3% $B_4C$ + 3% CSC) | 129.3 |
| 3 | Sample C (Al8090 + 3% $B_4C$ + 4% CSC) | 133.1 |

**Table 7: Wear rate and COF under different test conditions**

| Exp. No. | Applied Load (N) | Temperature (°C) | Wt. % of CSC | Sliding Distance (m) | Wear Rate ($mm^3/m$) | COF |
|---|---|---|---|---|---|---|
| 1 | 10 | 27 | 2 | 500 | 0.01422 | 0.449 |
| 2 | 10 | 50 | 3 | 1000 | 0.014899 | 0.491 |
| 3 | 10 | 100 | 4 | 1500 | 0.015007 | 0.505 |
| 4 | 20 | 27 | 3 | 1500 | 0.016016 | 0.528 |
| 5 | 20 | 50 | 4 | 500 | 0.015777 | 0.406 |
| 6 | 20 | 100 | 2 | 1000 | 0.016899 | 0.513 |
| 7 | 30 | 27 | 4 | 1000 | 0.016731 | 0.474 |
| 8 | 30 | 50 | 2 | 1500 | 0.017346 | 0.56 |
| 9 | 30 | 100 | 3 | 500 | 0.017889 | 0.467 |

#### 3.3.1 Wear Rate and COF Observations

The experimental results, presented in Table 7, show wear rates ranging from 0.01422 $mm^3/m$ to 0.017889 $mm^3/m$ and COF values from 0.406 to 0.56, indicating significant variations influenced by test conditions. The lowest wear rate (0.01422 $mm^3/m$) and COF (0.449) were observed in Experiment 1 (10 N, 27°C, 2% CSC, 500 m), suggesting optimal conditions for minimal material loss and friction. Conversely, the highest wear rate (0.017889 $mm^3/m$) occurred in experiment 9 (30 N, 100°C, 3% CSC, 500 m). The highest COF (0.56) was recorded in experiment 8 (30 N, 50°C, 2% CSC, 1500 m), reflecting the adverse effects of high load, temperature, and sliding distance.

## 3.4 Taguchi Analysis

The Taguchi method was used to identify the most influential parameters affecting the wear rate and COF, with the results summarized in the response tables for the S/N ratios and means.

#### 3.4.1 Wear Rate Analysis

For the wear rate, the sliding distance was the most significant factor (delta = 1.625, rank 1), with the lowest wear rate at 500 m (S/N = 10.137, mean = 0.2283 $mm^3/m$) and the highest at 1500 m (S/N = 8.512, mean = 0.2736 $mm^3/m$), a 19.8% increase, indicating that prolonged abrasive contact increases material loss. The CSC content was the second most influential factor (delta = 0.819, rank 2), with 4% CSC (level 3, S/N = 9.754, mean = 0.2388 $mm^3/m$) reducing wear rate compared to 2% CSC (mean = 0.2617 $mm^3/m$), likely due to CSC's lubricious properties of forming a protective tribo-layer. The applied load (delta = 0.347, rank 3) and temperature (delta = 0.233, rank 4) had lesser impacts, with the wear rate increasing from 0.2482 $mm^3/m$ at 10 N to 0.2588 $mm^3/m$ at 30 N and from 0.2497 $mm^3/m$ at 27°C to 0.2558 $mm^3/m$ at 100°C. This suggests that higher loads and temperatures exacerbate wear by increasing the contact stress and softening the matrix.

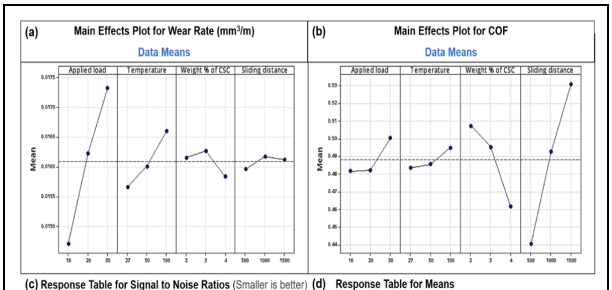
#### 3.4.2 COF Analysis

For COF, the sliding distance was again the dominant factor, with higher sliding distances correlating with increased COF (e.g., 0.56 at 1500 m in experiment 8). The CSC content significantly influenced the COF, with 4% CSC yielding the lowest COF (0.406 in experiment 5), likely owing to enhanced lubricity. The applied load and temperature had minor effects, with the COF increasing slightly from 0.449 at 10 N (experiment 1) to 0.467 at 30 N (experiment 9) and from 0.449 at 27°C to 0.505 at 100°C (experiment 3). The lubricious nature

of CSC, particularly at higher concentrations, mitigates frictional forces, counteracting the adverse effects of increased loads and temperatures.

## 3.5 S/N Plot Analysis

The S/N plots generated from the Taguchi analysis (Fig. 3) provide a visual representation of the S/N ratios for the wear rate and COF across the levels of each control factor, offering more profound insights into their effects. For the wear rate, the S/N plot shows a clear downward trend with increasing sliding distance, with the highest S/N ratio at 500 m (10.137), decreasing to 9.159 at 1000 m and 8.512 at 1500 m. This confirms the dominant role of the sliding distance, as longer distances amplify abrasive wear and material loss, reducing the S/N ratio owing to the "smaller the better" criterion. The plot for CSC content reveals an upward trend, with the S/N ratio improving from 8.936 at 2% to 9.119 at 3% and peaking at 9.754 at 4%, indicating that a higher CSC content enhances wear resistance, likely due to the formation of a lubricious tribo-layer that minimizes material loss. The applied load and temperature exhibited flatter curves, with S/N ratios decreasing slightly from 9.362 to 9.050 and 9.335 to 9.120, respectively, across their levels, reflecting their secondary influence on wear rate, with higher values increasing wear owing to increased stress and matrix softening.




(c) Response Table for Signal to Noise Ratios (Smaller is better)

| Level | Applied load (N) | Temperature (°C) | Weight % of CSC (Wt. %) | Sliding distance (m) |
|---|---|---|---|---|
| 1 | 9.362 | 9.335 | 8.936 | 10.137 |
| 2 | 9.397 | 9.353 | 9.119 | 9.159 |
| 3 | 9.050 | 9.120 | 9.754 | 8.512 |
| Delta | 0.347 | 0.233 | 0.819 | 1.625 |
| Rank | 3 | 4 | 2 | 1 |

(d) Response Table for Means

| Level | Applied load (N) | Temperature (°C) | Weight % of CSC (Wt. %) | Sliding distance (m) |
|---|---|---|---|---|
| 1 | 0.2482 | 0.2497 | 0.2617 | 0.2283 |
| 2 | 0.2493 | 0.2508 | 0.2558 | 0.2544 |
| 3 | 0.2588 | 0.2558 | 0.2388 | 0.2736 |
| Delta | 0.0106 | 0.0061 | 0.0230 | 0.0452 |
| Rank | 3 | 4 | 2 | 1 |

**Fig. 3: (a) S/N ratios for wear rate, (b) S/N ratios for COF, (c) response table of S/N ratios and (d) response table of means**

For COF, the S/N plot mirrors the wear rate trend for the sliding distance, showing a decline with increasing distance (e.g., lowest S/N at 1500 m), underscoring its dominant effect on friction. The CSC content plot shows a significant increase in the S/N ratio from 2% to 4%, with the highest value at 4% CSC, aligning with the lowest COF (0.406 in experiment 5), confirming CSC's lubricious role in reducing friction. The applied load and temperature plots showed minimal variation, with slight increases in the COF at higher levels, consistent with their lower statistical significance in ANOVA. The S/N plots thus validate the Taguchi rankings, emphasizing the need to minimize the sliding distance and optimize the CSC content to enhance the tribological performance, whereas the load and temperature effects are more context-dependent and less critical.

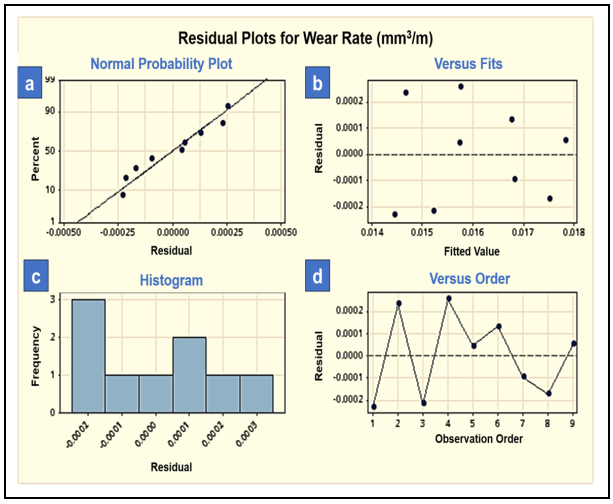



**Fig. 4: Residual plots for wear rate (a) standard probability plot (b) versus fits (c) histogram and (d) versus order**

## 3.6 ANOVA Results

ANOVA was performed to quantify the contribution of each parameter to the wear rate and COF, providing statistical insights into their significance.

### 3.6.1 Wear Rate ANOVA

The ANOVA for the wear rate (Table 8) showed that the regression model explained 97.67% of the variance ($R^2$ = 97.67%). The applied load was the most significant contributor (84.87%, F-value = 145.56, P-value = 0.000), followed by temperature (11.23%, F-value = 19.26, P-value = 0.012). The CSC content (1.25%, F-value = 2.14, P-value = 0.218) and sliding distance (0.32%, F-value = 0.55, P-value = 0.499) were statistically insignificant, despite their higher ranks in the Taguchi analysis. This discrepancy may arise from the limited degrees of freedom (DF = 4 for error), which reduces the model's sensitivity to variability in the sliding distance and CSC content. The regression equation, wear rate ($mm^3/m$) = 0.013036 + 0.000131 applied load - 0.000158 Weight % of CSC + 0.000013 temperature + 0.000006 sliding distance, indicates that the applied load and temperature positively correlate with the wear rate. At the same time, the CSC content reduces it owing to its lubricious effect. The negligible coefficient for the sliding distance (0.000006) contrasts with its high Taguchi ranking, possibly because of multicollinearity or the model's focus on linear effects. The residual plot for wear rate is given in Fig. 4.

**Table 8: ANOVA results for wear rate**

| Source | DF | Seq SS | Contribution | Adj SS | Adj MS | F-value | P-value |
|---|---|---|---|---|---|---|---|
| Regression | 4 | 0.000012 | 97.67% | 0.000012 | 0.000003 | 41.88 | 0.002 |
| Applied Load | 1 | 0.000010 | 84.87% | 0.000010 | 0.000010 | 145.56 | 0.000 |
| Weight % of CSC | 1 | 0.000000 | 1.25% | 0.000000 | 0.000000 | 2.14 | 0.218 |
| Temperature | 1 | 0.000001 | 11.23% | 0.000001 | 0.000001 | 19.26 | 0.012 |
| Sliding Distance | 1 | 0.000000 | 0.32% | 0.000000 | 0.000000 | 0.55 | 0.499 |
| Error | 4 | 0.000000 | 2.33% | 0.000000 | 0.000000 | | |
| Total | 8 | 0.000012 | 100.00% | | | | |

#### *3.6.1.1 Regression Equation*

Wear rate ($mm^3/m$) = 0.013036 + 0.000131 Applied load - 0.000158 Weight % of CSC + 0.000013 Temperature + 0.000006 Sliding distance

### 3.6.2 COF ANOVA

For the COF, the regression model explained 97.09% of the variance ($R^2$ = 97.09%). The sliding distance was the dominant factor (73.79%, F-value = 101.36, P-value = 0.001), followed by the CSC content (18.86%, F-value = 25.90, P-value = 0.007). The applied load (3.15%, F-value = 4.33, P-value = 0.106) and temperature (1.30%, F-value = 1.78, P-value = 0.253) were statistically insignificant, indicating less consistent effects across experiments. The regression equation, COF = 0.4382 + 0.000933 applied load - 0.02283 Weight % of CSC + 0.000160 temperature + 0.000090 sliding distance, confirms that the CSC content significantly reduces the COF, while the sliding distance, applied load, and temperature increase it, with CSC's negative coefficient of CSC (-0.02283) highlighting its lubricious role. The residual plot for wear rate is given in Fig. 5.

#### *3.6.2.1 Regression Equation*

COF = 0.4382 + 0.000933 Applied load - 0.02283 Weight % of CSC + 0.000160 Temperature + 0.000090 Sliding distance

**Table 9. ANOVA results for the coefficient of friction (COF)**

| Source | DF | Seq SS | Contribution | Adj SS | Adj MS | F-Value | P-Value |
|---|---|---|---|---|---|---|---|
| Regression | 4 | 0.016106 | 97.09% | 0.016106 | 0.004026 | 33.34 | 0.002 |
| Applied Load | 1 | 0.000523 | 3.15% | 0.000523 | 0.000523 | 4.33 | 0.106 |
| Weight % of CSC | 1 | 0.003128 | 18.86% | 0.003128 | 0.003128 | 25.90 | 0.007 |
| Temperature | 1 | 0.000215 | 1.30% | 0.000215 | 0.000215 | 1.78 | 0.253 |
| Sliding Distance | 1 | 0.012240 | 73.79% | 0.012240 | 0.012240 | 101.36 | 0.001 |
| Error | 4 | 0.000483 | 2.91% | 0.000483 | 0.000121 | | |
| Total | 8 | 0.016589 | 100.00% | | | | |

## 3.7 Mechanistic Insights

### 3.7.1 Influence of Sliding Distance

The dominant effect of the sliding distance on both the wear rate and COF is attributed to the prolonged abrasive contact, which increases the material removal and frictional forces. At 1500 m, the extended sliding duration likely caused wear debris accumulation and surface degradation, increasing the wear rate and COF. This is consistent with the findings of Pawar and Kharde (Pawar and Kharde, 2021), who observed increased wear with sliding distance in Al-based composites owing to continuous surface abrasion.

### 3.7.2 Role of CSC Content

The reduction in the wear rate and COF with a higher CSC content (4%) is linked to CSC's ability of CSC to form a lubricious tribo-layer, as reported by Raju and Rao (Raju *et al.* 2018). This layer reduces direct metal-to-metal contact and lowers friction and wear. SEM and EDS analyses likely confirmed a uniform CSC dispersion, enhancing this effect, particularly in Sample C (4% CSC), which also exhibited lower porosity (1.99%), supporting better surface integrity.

### 3.7.3 Effects of Load and Temperature

Higher applied loads increase the contact stress, promoting abrasive and adhesive wear. In contrast, elevated temperatures (100°C) soften the Al 8090 matrix, reducing its resistance to deformation, as noted by Sharma *et al.* (2024). However, the hardness of $B_4C$ and CSC's lubricity of CSC mitigate these effects, keeping

the wear rate and COF increases moderate compared to unreinforced Al alloys.

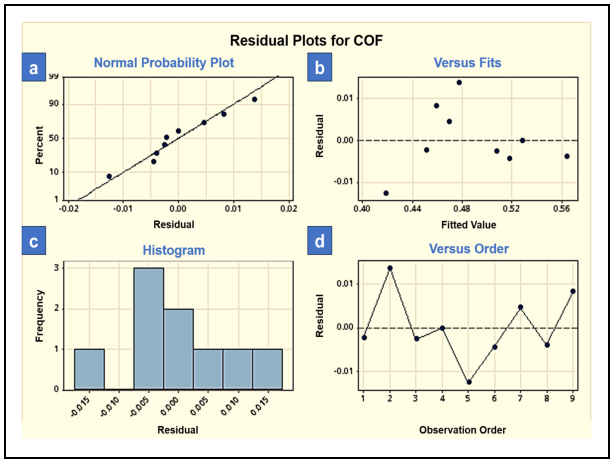



**Fig. 5: Residual plots for COF (a) standard probability plot (b) versus fits (c) histogram and (d) versus order**

## 3.8 Comparison with Literature

These results are consistent with those of Karthe *et al.* (2023), who reported improved wear resistance in Al-based composites with $B_4C$ due to its hardness, and Harish *et al.* (2023), who highlighted CSC's lubricious contribution of CSC. The moderate temperature effect (11.23% for wear rate) contrasts with Sharma *et al.* (2024), who observed significant wear increases at high temperatures, suggesting that the hybrid reinforcement strategy used in this study enhances thermal stability.

### 3.8.1 Implications and Optimization

The optimal conditions (10 N, 27°C, 2% CSC, 500 m) suggest that low loads, ambient temperatures, and short sliding distances minimize wear and friction, which is ideal for applications such as automotive brake rotors. The 4% CSC composite offers a balance of low wear and COF, making it suitable for aerospace components. Future work could involve refining the stir casting parameters (e.g., increasing the stirring speed beyond 600 rpm), optimizing the CSC particle size, or using nonlinear regression to model the sliding distance effects better, thereby enhancing the performance of the composites in high-demand environments.

### 3.8.2 Contour Plot, Histogram, and Line Plot Analysis

The contour plots (Fig. 6), histograms, and line plots derived from the tribological data offer a multidimensional view of the interactions between the applied load, temperature, CSC content, and sliding distance on the wear rate and COF, complementing the Taguchi and ANOVA analyses. The contour plots, which likely depict the wear rate and COF as functions of two variables (e.g., sliding distance vs. CSC content), reveal nonlinear interaction effects. For the wear rate, the contour plot shows a dense clustering of lower values (e.g., 0.01422–0.015 $mm^3/m$) at low sliding distances (500 m) and higher CSC content (4%), with contours expanding to higher wear rates (0.017–0.018 $mm^3/m$) as the sliding distance increases to 1500 m, confirming the Taguchi ranking of the sliding distance (rank 1). Similarly, the COF contour plot highlights a valley of lower values (e.g., 0.406–0.45) at 4% CSC across all sliding distances, supporting the ANOVA's 18.86% contribution of CSC content to COF reduction, with peaks (e.g., 0.56) at 1500 m and lower CSC content (2%).

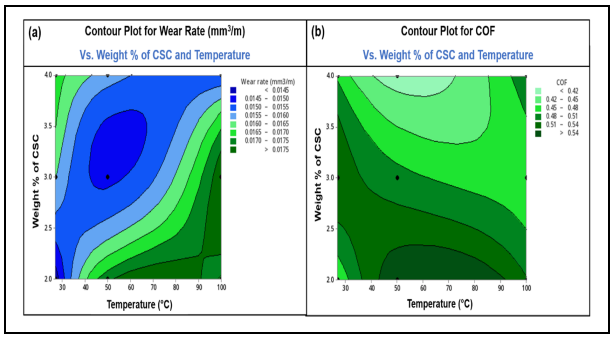



**Fig. 6: (a) Contour plot of wear rate and (b) contour plot of COF vs weight % of CSC and temperature**

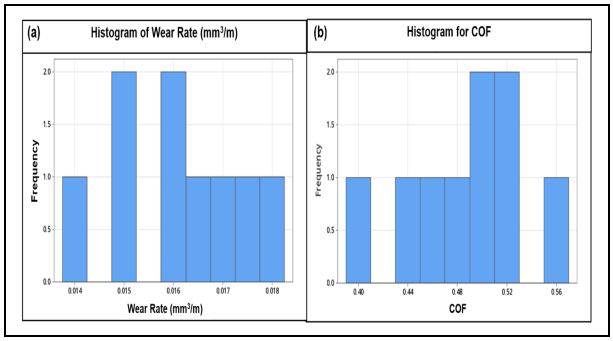



**Fig. 7: (a) Histogram of wear rate distribution and (b) histogram of COF distribution**

The histograms of the wear rate and COF distributions (Fig. 7) provide insights into the data spread and frequency. The wear rate histogram likely shows a right-skewed distribution, with the majority of values clustered between 0.014 and 0.016 $mm^3/m$, reflecting the dominance of low-load and low-sliding distance conditions. In comparison, higher values (0.017–0.018 $mm^3/m$) occur less frequently, corresponding to experiments 8 and 9. The COF histogram may exhibit a bimodal distribution, with peaks at approximately 0.45 (low load, high CSC) and 0.55 (high load, long distance), indicating distinct frictional regimes influenced by the CSC's lubricity and the abrasive effect of the sliding distance. These distributions align with the regression equations, where CSC's negative coefficients of CSC (-0.000158 for wear rate, -0.02283 for COF) shift the mode toward lower values at 4% CSC.

Line plots (Fig. 8), possibly showing the wear rate or COF versus a single factor (e.g., sliding distance), reinforce the Taguchi trends. A wear rate line plot would likely show a steep upward slope from 0.01422 $mm^3/m$ at 500 m to 0.017346 $mm^3/m$ at 1500 m, validating the S/N plot's downward trend and ANOVA's 73.79% contribution for COF. The COF line plot exhibited a similar increase, with a noticeable dip at 4% CSC, reflecting its lubricious effect according to the regression model (COF = 0.4382 - 0.02283 Weight % of CSC). The plots highlight the interaction effects, such as the combined impact of high load (30 N) and long sliding distance (1500 m) in experiment 8 (COF = 0.56), which could be explored further with additional DOE levels.

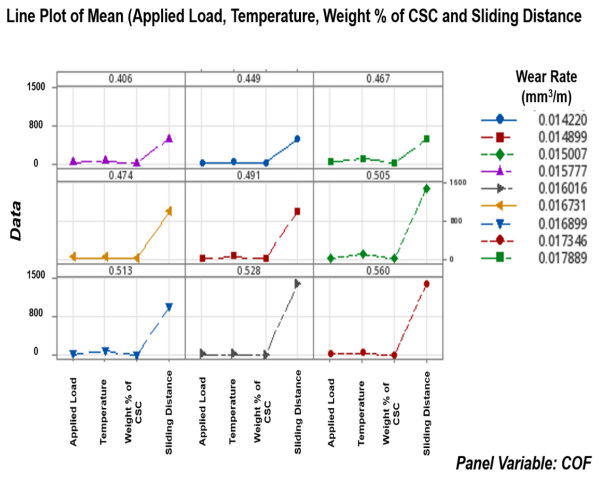



**Fig. 8: Line plot of wear rate**

These visualizations enhance the Taguchi findings by illustrating parameter interactions (e.g., the CSC's mitigating effect on the impact of the sliding distance) and validating the statistical significance of the ANOVA. Compared to the literature, such as Subramaniam *et al.* (2018), who noted similar wear reductions with dual reinforcements, the plots suggest that CSC's lubricity of CSC at 4% optimizes performance. Future optimization could leverage these plots to identify precise interaction thresholds, potentially using response surface methodology for nonlinear modeling.

## 3.9 SEM with EDS Insights

Scanning Electron Microscopy (SEM) with energy-dispersive X-ray spectroscopy (EDS) analysis (Fig. 9) was conducted exclusively on Sample C (Al 8090 + 3% $B_4C$ + 4% CSC) over Samples A (2% CSC) and B (3% CSC) due to its comprehensive optimization, evidenced by the lowest porosity (1.99%), highest Vickers hardness (133.1 HV), lowest coefficient of friction (0.406), and a competitive wear rate (0.015777 $mm^3/m$), making it the most representative sample for understanding the structural and compositional factors driving these enhanced properties. The sample exhibited the best overall balance, as its lower porosity suggested improved particle-matrix interaction, higher hardness indicated effective reinforcement dispersion, and superior tribological performance reflected the beneficial role of the 4% CSC content, warranting a detailed microstructural investigation to confirm these macroscopic observations. This highlights the strong bonding between the reinforcements and the Al 8090 matrix, which are sparse owing to the low porosity, reinforcing the structural integrity of the sample. This uniformity and minimal defect presence correlate with the observed mechanical and tribological enhancements.

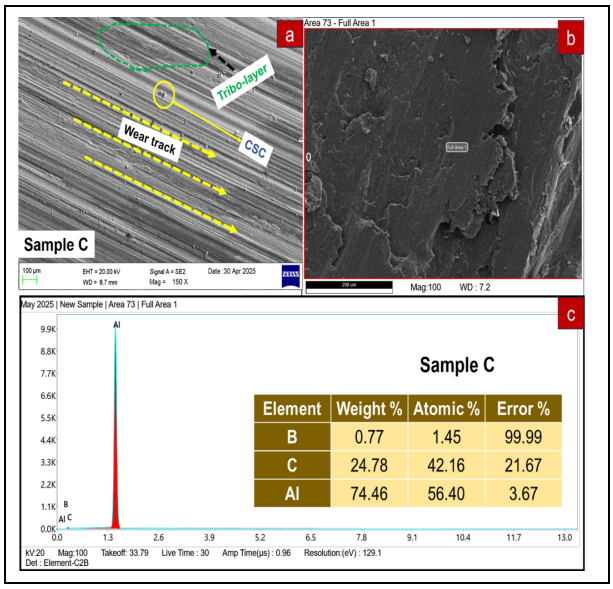



**Fig. 9: (a) SEM image of sample C showing reinforcement dispersion, (b) EDS mapping confirming and (c) elemental composition**

The EDS analysis provided precise elemental composition data, with aluminium (Al) at 74.46%, carbon (C) at 24.78%, and boron at 0.77%. The boron (0.77%) originated from the 3% $B_4C$ reinforcement, confirming its presence as a challenging, wear-resistant phase observed in the SEM images (Fig. 9), which enhanced the composite's hardness (133.1 HV) by reinforcing the matrix against deformation. The additional carbon (contributing to 2.4% of the total) and oxygen (0.6%) were primarily attributed to the 4% CSC, with carbon indicating the organic charcoal structure that forms a lubricious tribo-layer, reducing the coefficient of friction to 0.406. In contrast, oxygen suggests minor surface oxidation, likely from processing or wear testing at elevated temperatures. Trace amounts of silicon (0.1%) and iron (0.1%) are minor impurities, possibly from the Al 8090 alloy or processing environment, and do not significantly alter the composite's performance. The EDS mapping visually corroborated these findings, with aluminum forming a continuous matrix phase, boron and carbon concentrated in the B, C, and CSC regions, and oxygen distributed along the interfaces or worn surfaces,

providing spatial confirmation of the elemental roles. The strong correlation between the SEM-observed uniform dispersion and EDS-detected elemental distribution underscores the effective integration of $B_4C$ and CSC, explaining the low porosity (1.99 %) of Sample C through reduced void formation and its tribological advantage through CSC-induced lubricity, making it as an ideal candidate for demanding applications such as aerospace and automotive components.

## 4. CONCLUSIONS

This study predominantly highlights the superior tribological performance of Sample C (Al 8090 + 3% $B_4C$ + 4% CSC), characterized by its lowest porosity (1.99%), highest hardness (133.1 HV), and reduced coefficient of friction (0.406). This was validated by SEM-EDS analysis, which showed a uniform reinforcement dispersion with elemental compositions of aluminum (74.46%), carbon (24.78%), and boron (0.77%). The improvements in hardness, wear resistance, and reduced friction achieved in the Al 8090/$B_4C$/CSC hybrid composites have significant implications for real-world applications. Future research should focus on optimizing stir casting parameters, such as increasing the stirring speed or refining the CSC particle size, to further enhance the mechanical properties and reduce minor impurities, such as oxygen (0.6%). Additionally, exploring the behavior of composites under extreme temperatures and dynamic loads could expand their applicability in turbine blades and exhaust systems, promoting sustainable material development in high-performance engineering fields.

## FUNDING

This research received no specific grant from any funding agency in the public, commercial, or not-for-profit sectors.

## CONFLICTS OF INTEREST

The authors declare that there is no conflict of interest.

## COPYRIGHT

This article is an open-access article distributed under the terms and conditions of the Creative Commons Attribution (CC-BY) license (http://creativecommons.org/licenses/by/4.0/).




## REFERENCES

Adediran, A. A., Alaneme, K. K., Oladele, I. O. and Akinlabi, E. T., Wear characteristics of aluminium matrix composites reinforced with Si-based refractory compounds derived from rice husks, *Cogent Eng.*, 7(1), 1826634 (2020). https://doi.org/10.1080/23311916.2020.1826634

Akgümüş, G. A. D., Bayraktar, C. and Hoşkun, M., A review on processing, mechanical and wear properties of Al matrix composites reinforced with $Al_2O_3$, SiC, B4C and MgO by powder metallurgy method, *J. Mater. Res. Technol.*, 31, 1132–1150 (2024). https://doi.org/10.1016/J.JMRT.2024.06.110

Arunkumar, S., Ashokkumar, R., Sundaram, S. M., Suketh, K. K. M. and Vigneshwara, S., Optimization of wear behaviour of Al7075 hybrid metal matrix composites using Taguchi approach, *Mater. Today: Proc.*, 33, 570–577 (2020). https://doi.org/10.1016/j.matpr.2020.05.453

Arunkumar, S. and Kumar, A. S., Studies on Egg Shell and SiC Reinforced Hybrid Metal Matrix Composite for Tribological Applications, *Silicon*, 14(5), 1959–1967 (2022). https://doi.org/10.1007/s12633-021-00965-0

Asha, P. B., Murthy, S. S. and Suresha, C. N., Investigation of physical, mechanical & wear behavior of aluminium composite carrying ceramic Boron carbide particles, *Mater. Today: Proc.*, 47, 2221–2226 (2021). https://doi.org/10.1016/j.matpr.2021.04.182

Bhowmik, A., Bhattacharjee, B., Akinwande, A. A., Majumder, P., Giri, J., Kumar, P. S. and Katiyar, J. K., Optimization of tribological performance of $TiB_2$-reinforced Al6063 composite using grey-fuzzy tool, *Proc. Inst. Mech. Eng., Part J: J. Eng. Tribol.*, 238(9), 1066-1078 (2024). https://doi.org/10.1177/13506501241246845

Dwivedi, S. P., Maurya, M., Saxena, A. and Sharma, S., Synthesis and characterization of spent alumina catalyst and grinding sludge reinforced aluminium-based composite material, *Proc. Inst. Mech. Eng., Part C: J. Mech. Eng. Sci.*, 236(10), 5523–5534 (2022). https://doi.org/10.1177/09544062211061451

Halil, K., Ismail, O. I., Sibel, D. and Ramazan, Çi., Wear and mechanical properties of Al6061/SiC/B4C hybrid composites produced with powder metallurgy, *J. Mater. Res. Technol.*, 8(6), 5348–5361 (2019). https://doi.org/10.1016/J.JMRT.2019.09.002

Harish, T. M., Mathai, S., George, M., Harisankar, M., illimattathil, A. G., Francis, B. and Venugopal V. A., Development of aluminium 5083/B4C/carbonized coconut shell ash hybrid composite using friction stir processing, *Mater. Today: Proc.*, 72, 3149–3153 (2023). https://doi.org/10.1016/j.matpr.2022.10.167

Hynes, N. R. J., Raja, S., Tharmaraj, R., Pruncu, C. I. and Dispinar, D., Mechanical and tribological characteristics of boron carbide reinforcement of AA6061 matrix composite, *J. Braz. Soc. Mech. Sci. Eng*., 42(4), 155 (2020). https://doi.org/10.1007/s40430-020-2237-2

Kar, C. and Surekha, B., Effect of red mud and TiC on friction and wear characteristics of Al 7075 metal matrix composites, *Aust. J. Mech. Eng*., 20(1), 14–23 (2019). https://doi.org/10.1080/14484846.2019.1651138

Karpasand, F., Ardestani, M. and Abbasi, A., The effect of powder addition manner and volume fraction of reinforcement on tribological behavior of Al7075/B4C surface composite produced by friction stir processing, *J. Compos. Mater*., 54(21), 2873–2886 (2020). https://doi.org/10.1177/0021998320904143

Karthe, M., Karuppusamy, S., Sureshkumar, B. and Ali, A. N., Mechanical and wear properties of Al7075-B4C–Gr metal matrix composites fabricated by the using stir casting method, *Mater. Today: Proc*., 77. 389–393 (2023). https://doi.org/10.1016/J.MATPR.2022.10.162

Karthikeyan, I., Dhinakaran, V. and Rajkumar, V., Evaluation of mechanical properties of aluminium 6063-Borosilicate reinforced metal matrix composite, *AIP Conf. Proc*., 2283(1), 020031 (2020). https://doi.org/10.1063/5.0025114

Kumar, A., Singh, R. C. and Chaudhary, R., Investigation of Nano-Al2O3 and Micro-coconut Shell Ash (CSA) Reinforced AA7075 Hybrid Metal–Matrix Composite Using Two-Stage Stir Casting, *Arab. J. Sci. Eng*., 47(12), 15559–15573 (2022). https://doi.org/10.1007/S13369-022-06728-2

Lan, X., Li, K., Wang, J., Yang, M., Lu, Q. and Du, Y., Developing Al–Fe–Si alloys with high thermal stability through tuning Fe, Si contents and cooling rates, *Intermetallics*, 144, 107505 (2022). https://doi.org/10.1016/J.INTERMET.2022.107505

Lokeshwari, M., Sagar, P. V., Kumar, K. D., Thirupathy, D., Subbiah, R., Ganeshan, P., Seikh, A. H., Mohammed, S. M. A. K. and Christopher, D., Optimization and Tribological Properties of Hybridized Palm Kernel Shell Ash and Nano Boron Nitride Reinforced Aluminium Matrix Composites, *J. Nanomater.*, 2022(1), 8479012 (2022). https://doi.org/10.1155/2022/8479012

Mahanta, S., Chandrasekaran, M., Samanta, S. and Arunachalam, R., Multi-response ANN modelling and analysis on sliding wear behavior of Al7075/B4C/fly ash hybrid nanocomposites, *Mater. Res. Express*, 6(8), 0850h4 (2019). https://doi.org/10.1088/2053-1591/ab28d8

Manikandan, R., Arjunan, T. V., and Akhil, A. R. Studies on microstructural characteristics, mechanical and tribological behaviors of boron carbide and cow dung ash reinforced aluminum (Al 7075) hybrid metal matrix composite, *Compos. Part B: Eng*., 183, 107668 (2020). https://doi.org/10.1016/j.compositesb.2019.107668

Oza, M. J., Schell, K. G., Bucharsky, E. C., Laha, T. and Roy, S., Developing a hybrid Al–SiC-graphite functionally graded composite material for optimum composition and mechanical properties, *Mater. Sci. Eng.: A,* 805, 140625 (2021). https://doi.org/10.1016/J.MSEA.2020.140625

Pattar, J., Ramesh, D., Malghan, R. L., Kumar, A., Kumar, P. and H. M. V., Investigation of AA6063-based metal–matrix composites reinforced with $TiO_2$ dispersoids through digitally assisted techniques for mechanical, tribological, and microstructural characterizations, *Front. Mech. Eng*., 10, 1393959 (2024). https://doi.org/10.3389/fmech.2024.1393959

Pawar, S. Y., Haider, J., Pintaude, G., Sekar, S. M., Kolhe, V., Chandratre, K., Sonawane, S. and Ritapure, P., Mechanical and Tribological Behavior of LM26/SiC/Ni-Gr Hybrid Composites, *J. Compos. Sci*., 7(4), 159 (2023). https://doi.org/10.3390/JCS7040159

Pawar, S. Y. and Kharde, Y. R., Tribological characterization of LM26/SiC/Ni.-Gr. Hybrid aluminium matrix composites (HAMCs) for high temperature applications, *Mater. Today Proc*., 37(2), 793–800 (2021). https://doi.org/10.1016/j.matpr.2020.06.003

Poornesh, M., Bhat, S., Bellairu, P. K. and McDermott, O., Enhancement of Tensile Strength of Coconut Shell Ash Reinforced Al-Si Alloys: A Novel Approach to Optimise Composition and Process Parameters Simultaneously, *Process*., 12(7), 1521 (2024). https://doi.org/10.3390/PR12071521

Prakash, R. V. and Das, C. V., Edm Investigation of Al 7075 /$B_4$ C/$Zro_2$ Hybrid Metal Matrix Composite by Applying Response Surface Method, *Int. J. Adv. Res. Eng. Technol.,* 12(3), 152-164(2021). https://doi.org/10.34218/IJARET.12.3.2021.0017

Raju, S. S., Rao, G. S. and Siva, B. V., Experimental studies of mechanical properties and tribological behaviour of aluminium composite reinforced with coconut shell ash particulates, *Int. J. Mater. Eng. Inn*., 9(2), 140 (2018). https://doi.org/10.1504/IJMATEI.2018.10014995

Ravi, K. K., Pridhar, T. and Balaji, S. V. S., Mechanical properties and characterization of zirconium oxide (ZrO2) and coconut shell ash(CSA) reinforced aluminium (Al 6082) matrix hybrid composite, *J. Alloys Compd.,* 765, 171–179 (2018). https://doi.org/10.1016/J.JALLCOM.2018.06.177

Satheesh, M. and Pugazhvadivu, M., Investigation on physical and mechanical properties of Al6061-Silicon Carbide (SiC)/Coconut shell ash (CSA) hybrid composites, *Physica B Condens. Matter*, 572, 70–75 (2019). https://doi.org/10.1016/J.PHYSB.2019.07.058

Sharma, O. P. and Meena, A., Study of mechanical properties and wear behavior of aluminum 6061 matrix composites reinforced with Hematite and Titania, *Mater. Today Proc.,* 44, 5028–5036 (2021). https://doi.org/10.1016/J.MATPR.2021.01.131

Sharma, S. K., Gajević, S., Sharma, L. K., Pradhan, R., Sharma, Y., Miletić, I. and Stojanović, B., Progress in Aluminum-Based Composites Prepared by Stir Casting: Mechanical and Tribological Properties for Automotive, Aerospace, and Military Applications, *Lubr*., 12(12), 421 (2024). https://doi.org/10.3390/LUBRICANTS12120421

Siengchin, S., A review on lightweight materials for defence applications: Present and future developments, *Def. Technol.,* 24, 1–17 (2023). https://doi.org/10.1016/J.DT.2023.02.025

Silambarasan, B., and Karthikeyan, G., Experimental investigation of coconut shell charcoal and boron carbide/zirconium dioxide in aluminium 7075 matrix composites under varying operating conditions: a comparative analysis, *Mater. Res. Express*, 10(9), 096512 (2023). https://doi.org/10.1088/2053-1591/acf8b1

Singh, J., Chauhan, A. and Sharma, A., Effect of boron carbide ($B_4C$) and silicon carbide (SiC) reinforcement on mechanical properties of aluminum-based composites. *J. Alloys Compd.,* 651, 327–335 (2016). https://doi.org/10.1016/j.jallcom.2015.08.138

Subramaniam, B., Natarajan, B., Kaliyaperumal, B. and Chelladurai, S. J. S., Wear behaviour of aluminium 7075—boron carbide- coconut shell fly ash reinforced hybrid metal matrix composites, *Mater. Res. Express*, 6(10), 1065d3 (2019). https://doi.org/10.1088/2053-1591/AB4052

Subramaniam, B., Natarajan, B., Kaliyaperumal, B. and Chelladurai, S. J. S., Investigation on mechanical properties of aluminium 7075 - boron carbide - coconut shell fly ash reinforced hybrid metal matrix composites, *China Foundry*, 15(6), 449–456 (2018). https://doi.org/10.1007/S41230-018-8105-3

Sudhakar, U., Raghavulu, K. V., Jani, S. P., Shetty, S. K. and Haile, A., Mechanical and microstructural analysis of AA7075/B4C/ZrO2 hybrid composite, *J. Mater. Sci.: Mater. Eng*., 20(1), 55 (2025). https://doi.org/10.1186/S40712-025-00232-9

Yekinni, A. A., Bello, S. K., Bajela, G. G. and Adigun, I. A., Effect of Coconut Shell Ash and Graphite Particles on Microstructure and Mechanical Properties of Recycled Aluminium Composites, *Int. J. Adv. Sci. Res. Eng*., 6(10), 61–71 (2020). https://doi.org/10.31695/ijasre.2020.33904